Journal of Power Sources 247 (2014) 228–234

Contents lists available at ScienceDirect

Journal of Power Sources

journal homepage: www.elsevier.com/locate/jpowsour

Effects of carbon brush anode size and loading on microbial fuel cell performance in batch and continuous mode

Vanessa Lanas, Yongtae Ahn, Bruce E. Logan*

Department of Civil & Environmental Engineering, Penn State University, 212 Sackett Building, University Park, PA 16802, USA

HIGHLIGHTS

- The location of the geometric center of mass of the anode had a significant effect on power output.
- At equal position of the geometric center of the anode, larger brushes perform better.
- Power densities, COD removal and CE were lower in continuous flow operation.
- Smaller brush diameters enable closer spacing and the design of more compact reactors.

GRAPHICAL ABSTRACT

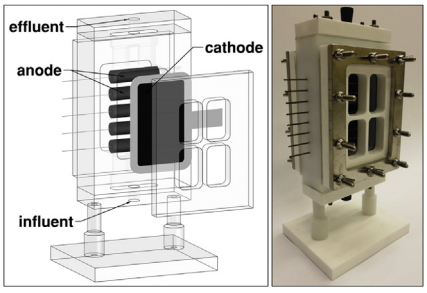

ARTICLE INFO

Article history:
Received 2 July 2013
Received in revised form
27 August 2013
Accepted 27 August 2013
Available online 4 September 2013

Keywords:
Microbial fuel cell
Carbon brush anode
Diameter
Electrode distance
Continuous flow

ABSTRACT

Larger scale microbial fuel cells (MFCs) require compact architectures to efficiently treat wastewater. We examined how anode-brush diameter, number of anodes, and electrode spacing affected the performance of the MFCs operated in fed-batch and continuous flow mode. All anodes were initially tested with the brush core set at the same distance from the cathode. In fed-batch mode, the configuration with three larger brushes (25 mm diameter) produced 80% more power (1240 mW m^{-2}) than reactors with eight smaller brushes (8 mm) (690 mW m^{-2}). The higher power production by the larger brushes was due to more negative and stable anode potentials than the smaller brushes. The same general result was obtained in continuous flow operation, although power densities were reduced. However, by moving the center of the smaller brushes closer to the cathode (from 16.5 to 8 mm), power substantially increased from 690 to 1030 mW m^{-2} in fed batch mode. In continuous flow mode, power increased from 280 to 1020 mW m^{-2}, resulting in more power production from the smaller brushes than the larger brushes (540 mW m^{-2}). These results show that multi-electrode MFCs can be optimized by selecting smaller anodes, placed as close as possible to the cathode.

1. Introduction

Microbial fuel cells (MFCs) are bioelectrical devices that use microorganisms to oxidize the organic matter present in wastewaters from different sources (domestic, industrial, agricultural), and generate electrical power that can be harvested for numerous purposes [1–3]. Current efforts in ongoing MFC research are directed towards improving the efficiency of this process to make it economically and commercially feasible. Significant advances have been made in understanding microbial exoelectrogenic communities, electrochemical reaction kinetics [4], and the economic feasibility of the process based on reactor materials [5]. Application of MFCs for wastewater treatment will require the design of compact reactors, the use of inexpensive materials, and a better

* Corresponding author. Tel.: +1 814 863 7908.
E-mail address: blogan@psu.edu (B.E. Logan).

0378-7753/$ – see front matter © 2013 Elsevier B.V. All rights reserved.
http://dx.doi.org/10.1016/j.jpowsour.2013.08.110

understanding of how to achieve optimum conditions for power generation [6]. Electrode design is critical given the need for larger power production and the contribution of the materials used to overall reactor cost [7]. Carbon brush anodes are ideal for scaling-up MFCs as they have large porous surface areas, are relatively noncorrosive, have low resistance and good electrical conductivity, and show a compact and structured distribution of the bristles that helps to avoid biofouling [8].

The use of multiple brush anodes has proven to be effective for building larger-scale MFCs in the laboratory [9–11] as long as large changes in substrate concentrations within the reactor are avoided under continuous flow conditions [12–15]. A multi-anode system based on a separator electrode assembly design was tested in both batch and continuous regime [16]. Power production reached 975 mW m^{-2} in fed-batch mode using acetate, and 880 mW m^{-2} in continuous flow operation with a hydraulic retention time (HRT) of 8 h that avoided very large changes in substrate concentrations. These reactors contained separators so that the anodes could be placed close to the cathode, but separators can reduce performance as they increase reactor internal resistance. MFCs can be designed so that separators are not needed by positioning the anodes so that they do not make contact with the cathode. With this configuration, the minimum chamber width is equal to that of the diameter of the brush. Decreasing the size of the brush could therefore enable the construction of more compact reactors.

The size of the anode brush has not been systematically investigated with respect to reactor performance. The effect of brush size has only been studied for brushes placed perpendicular to the cathode [17]. In this orientation, it was shown that reducing the mass of the graphite fiber brush distant from the cathode (by trimming the brush length) did not affect performance until more than 65% of the brush mass was removed. This suggested that the brushes might be more optimally designed with respect to their size. In order to better understand the effect of the brush diameter on MFC performance, MFCs with multiple anodes were constructed with a variable number of brushes (3, 5 or 8). The projected area of these brushes relative to the cathode was kept relatively constant by using more brushes with smaller diameters. The performance of the MFCs was examined in terms of maximum power generation, substrate removal, and coulombic efficiency (CE) in both fed-batch and continuous flow modes of operation.

2. Materials and methods

2.1. Construction

The main reactor body of the MFC was made of high density polyethylene (HDPE) as previously described [16], but no separator was used, and the anode sizes and placement were varied (Fig. 1). The brush anodes were designed to fully span the width of the anode chamber, with the brushes placed parallel to the cathode, in the middle of the anode chamber (95 × 142 × 38 mm, 174 ± 3 mL), except as noted. The anodes were connected externally in parallel by a single copper wire. Three different sized anodes were made using carbon fibers (PANEX 35 50K, Zoltek) wound into two twisted titanium wires (length = 95 mm, diameter = 0.8 mm, gauge 20) (made by Mill-Rose) (Fig. S1). The anode sizes were: 3 brushes each 25 mm in diameter, with an electrode space (between the brush edge and the cathode) of 4 mm (R3; Fig. 2A); 5 brushes each 12 mm in diameter with an electrode space of 10 mm (R5; Fig. 2B); and 8 brushes each 8 mm in diameter, with an electrode space of 12 mm (R8; Fig. 2C). The R8 configuration was modified in a subsequent experiment by moving the anodes closer to the cathode (R8C), so that the gap between the anode edge and the cathode was the same as that of the R3 configuration (4 mm). All anodes were heat treated for 30 min at 450 °C [18] before inoculation.

Anode specific surface areas varied due to the differences in geometries (Table 1). Surface areas were calculated in several different ways. The cylinder-equivalent projected area, that includes the ends and the main cylinder surface, was calculated as $(2\pi r^2 + 2\pi rh)n$, where r is the brush radius, h the brush length, and n the total number of brushes. The specific bristle area was calculated as the external area of each bristle multiplied by the number of bristles per brush and by the total number of brushes. Each of these areas was normalized by the anolyte volume or the cathode surface area. The percentage of the cathode covered by the projected area of the brushes was calculated from the two dimensional area of the brush (rh) multiplied by the number of brushes, and divided by the cathode surface area.

A single air-cathode 35 cm^2 in projected area (5 × 7 cm) was used, producing a cathode-specific surface area of 20 m^2 m^{-3}. Air-cathodes were made from wet-proofed (30%) carbon cloth (Type B-1B, E-TEK), coated with carbon black, platinum (0.5 mg Pt/cm^2) and Nafion binder on the electrolyte-facing side, and carbon black base layer and four PTFE diffusion layers on the air-facing side [19]. A titanium shim pressed against the cathode was used as cathode current collector. An Ag/AgCl reference electrode (RE-5B, BASi) was placed laterally in each reactor in contact with the electrolyte to measure electrode potentials. There was no separator as the distance between the brushes and the cathode prevented electrical contact.

2.2. Inoculation and operation

The medium consisted of sodium acetate (1.0 g L^{-1}) in a 50 mM phosphate buffer nutrient solution (PBS) prepared with Na_2HPO_4 (4.58 g L^{-1}), $NaH_2PO_4 \cdot H_2O$ (2.45 g L^{-1}), NH_4Cl (0.31 g L^{-1}), KCl (0.13 g L^{-1}), trace minerals (12.5 mL L^{-1}), and vitamins (5 mL L^{-1}) (solution conductivity of 7.8 mS cm^{-1}, pH = 7) [20]. MFCs were inoculated with a 50% (v/v) effluent from reactors that operated for over a year, and 50% PBS with 1 g L^{-1} acetate. Steady state operation was achieved based on repeatable peak potentials for at least three consecutive cycles. After acclimation, only PBS plus acetate was added, with the solution replaced when the voltage decreased to <20 mV. The reactors were operated with an external circuit connected to a 1000 Ω resistor except as noted. The potential difference was measured every 20 min intervals using a multimeter (Keithley Instruments, model 2700) and recorded on a personal computer.

2.3. Experimental set-up

Polarization and power density curves were obtained using multi-cycle and single-cycle methods. The single-cycle method was performed after adapting the reactors to a low external resistance of 10 Ω to minimize the potential for power overshoot [21]. For fed-batch tests, the reactors were operated for at least three cycles at the different external resistances (1000 Ω–10 Ω) to fully acclimate the biofilms and ensure reproducible cycles of voltage generation. The recorded voltage at each resistance was based on the average over 2 h. For continuous flow tests, the HRT was set at 8 h [16], with flow (0.36 mL min^{-1}) from the bottom to the top of the reactor set using a peristaltic pump (Masterflex, Cole-Parmer).

2.4. Data analysis

Current (I) and power (P) were calculated as previously described [22], and normalized by the projected cathode surface area [23]. Chemical oxygen demand (COD) removal was obtained as the proportional difference between influent and effluent CODs

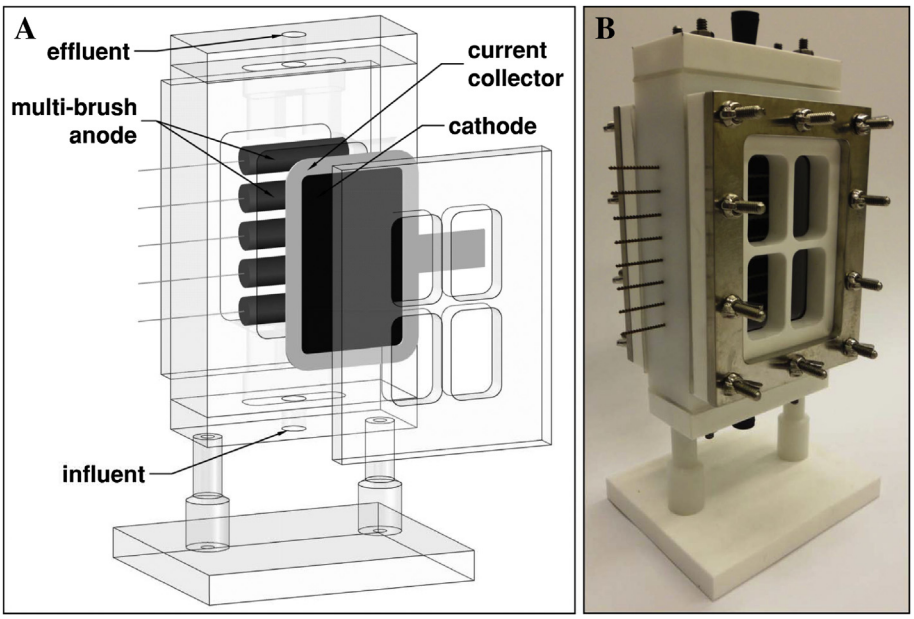

Fig. 1. Rectangular vertical MFC: (A) schematic design of R5 displaying front parts, and (B) photography of R8 completely assembled, showing air-cathode. The reactors are held together by stainless steel bolts and covered by a stainless steel frame for a water tight seal.

measured using standard methods (Standard Method 5220, APHA 1995, high range 20–1500 mg L^{-1}, low range 3–150 mg L^{-1}; HACH COD System, Hach Company, Loveland, Colorado) [20,24]. CE (%) was calculated as $CE = (C_{ex}/C_{th}) \times 100$. C_{ex} is the actual charge (C) collected by the anode during one batch cycle, $C_{ex} = \sum_{1}^{t} (U_i T_i)/R$, where U is voltage (V), T is time (s) and R is the external resistance (Ω). C_{th} is the theoretical amount of coulombs available from the oxidation of acetate to CO_2, calculated [23] as $C_{th} = (FbCOD_{in}v)/M$, where F is the Faraday's constant (96,485 C mol^{-1} e^-), b the number of moles of electrons exchanged per mole of oxygen (4 mol e^- mol^{-1} O_2), COD_{in} is the influent COD (g L^{-1}), v is the medium volume (0.028 L) and M is the molar weight of oxygen (32 g mol^{-1}).

Impedance was calculated from measurements by linear sweep voltammetry (LSV) or electrochemical impedance spectroscopy (EIS), with a potentiostat (BioLogic, VMP3). Both electrochemical experiments were performed at OCP, with the anode as working electrode and the cathode as the counter and reference electrode. After 2 h at 10 Ω and 30 min at OCP, LSV was performed at a slow scan rate of 0.1 mV s^{-1} [25], from −500 mV to −50 mV. The total internal resistance (R_{int}) was calculated as the slope of the linear portion of the polarization curve, or $R_{int} = \Delta U/\Delta I$ [23]. EIS was conducted over a frequency of 100 kH–2 mHz with sinusoidal perturbation of 10 mV in amplitude. The components of internal resistance were obtained by analyzing Nyquist and Bode plots with EC-Lab V10.02 software. Solution resistance was identified as the point where the impedance data crosses the x-axis [15,26], with charge transfer resistance calculated as the diameter of the first semicircle [27] in a Nyquist plot. Diffusion resistance was obtained from the lowest frequency plateau in the Bode plot [17]. Resistivity (ρ, Ω cm) was obtained as $\rho = RA/L$, where A is the cathode area (35 cm^2), L is the distance between the cathode and the center of

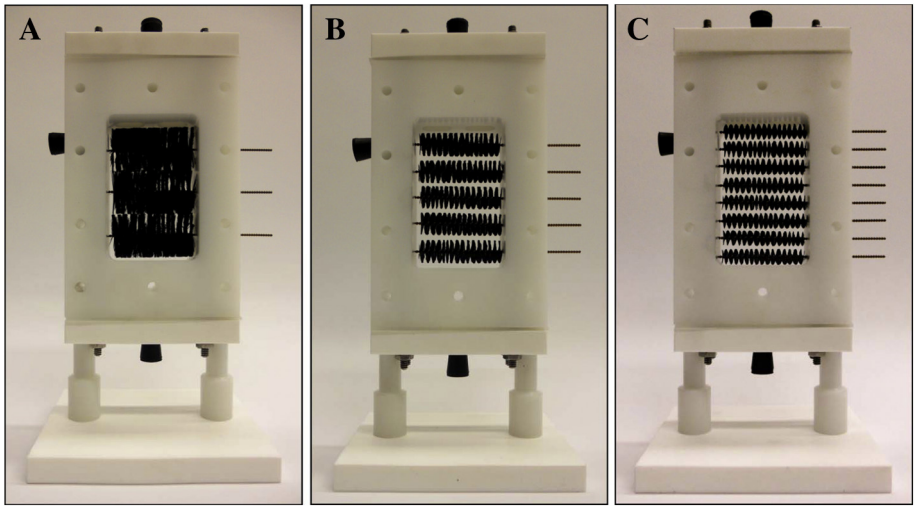

Fig. 2. Three vertical rectangular MFC configurations showing the different brushes used as anodes: (A) R3 has three brush anodes, (B) R5 has five brush anodes, and (C) R8 has eight brush anodes.

Table 1
Normalized anode surface areas and electrode space.

Area	Units	R3	R5	R8	R8C
Cylindrical area all brushes/anolyte	$m^2\ m^{-3}$	81	56	56	56
Specific bristle area all brushes/anolyte	$m^2\ m^{-3}$	3459	2750	2912	2912
Cylindrical area all brushes/cathode	$m^2\ m^{-2}$	3.4	2.5	2.5	2.5
Specific bristle area all brushes/cathode	$m^2\ m^{-2}$	147	120	130	130
Projected area brushes/cathode	%	99	79	84	84
Electrode spacing (brush edge)	mm	4	10.5	12.5	4
Electrode spacing (geometrical center)	mm	16.5	16.5	16.5	8

mass of the anode (1.7 cm for R3, R5 and R8; 0.8 cm for R8C), and R is the resistance (Ω).

3. Results and discussion

3.1. Maximum power densities in fed-batch and continuous flow modes

Maximum power density curves obtained when the MFCs were operated in fed-batch mode indicated substantial differences among the three anode configurations. The maximum power density was highest for the R3 configuration, with 1270 mW m^{-2} (0.32 mA cm^{-2}) based on single cycle test results (Fig. 3A). The maximum power produced decreased when more brushes were used, to 910 mW m^{-2} (0.29 mA cm^{-2}) for R5, and 600 mW m^{-2} (0.23 mA cm^{-2}) for R8. Maximum power densities obtained in multi-cycle tests [22] were quite similar (Fig. S1). Analysis of the electrode potential curves (Fig. 3B) showed that the current drop was mainly a result of reduced anode performance, as the potentials rapidly increased at the higher current densities.

When reactors were operated in continuous flow mode, the maximum power densities were all lower, with slightly different results in terms of which anode configuration was optimal. The R3 and R5 configurations produced about the same maximum power densities, with 560 mW m^{-2} (0.22 mA cm^{-2} at 30 Ω) for R3, and 600 mW m^{-2} (0.36 mA cm^{-2} at 10 Ω) for R5. The lowest power density of 280 mW m^{-2} (0.13 mA cm^{-2} at 50 Ω) was again obtained by the R8 configuration (Fig. 3C). These power densities are lower than those obtained in fed-batch mode, consistent with previous studies [16]. The maximum power densities obtained by configuration R3 here were similar to those reported by Ahn and Logan [16], even though they used three slightly shorter anodes in a separator electrode assembly design (SEA). They obtained 975 mW m^{-2} in fed-batch mode, and 880 mW m^{-2} in continuous mode at the same HRT (8 h). Several factors contribute to a lower power density in continuous vs. fed-batch mode operation, but it is most likely due to the lower average COD concentration in the reactor at an HRT of 8 h, compared to the higher COD concentration at the beginning of a fed-batch cycle (see below). One unexpected result from the continuous flow operation was that cathode performance appeared to be the main cause of the reduced voltage, as the cathode potentials became negative at higher current densities while the anode potential remained almost constant (Fig. 3D). This result could be an artifact of the placement of the reference electrode at a distance too far from the brush anodes. It was not considered likely that the cathode performance would change as there was no alteration of its structure or location.

3.2. COD removal and CE

COD removal was decreased in continuous mode (above 85% in batch mode vs. 14–45% in continuous flow mode) (Fig. 4A and C),

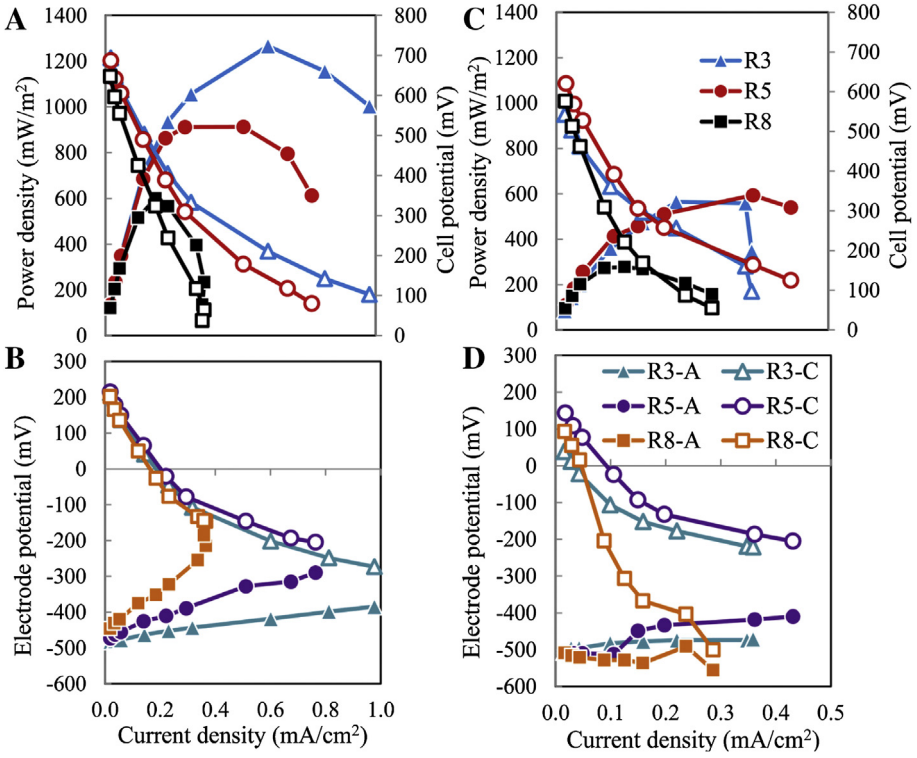

Fig. 3. (A and C) Power density (solid symbols) and polarization curves (white symbols) for MFCs obtained using the single-cycle method with three configurations: R3 (Δ), R5 (○), and R8 (□). (B and D) Electrode potential curves (A = anode, solid symbols; and C = cathode, white symbols) measured against a reference electrode (Ag/AgCl). The curves were obtained in fed-batch (A, B) and continuous flow (C, D) operation.

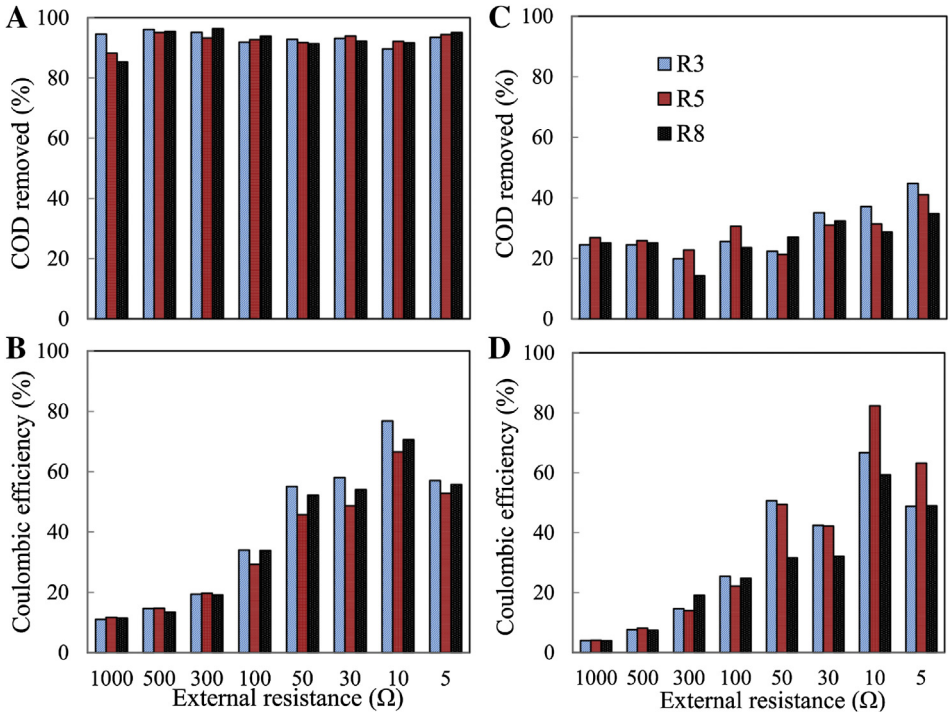

Fig. 4. COD removal (A, C) and Coulombic efficiency (B, D) in fed-batch (A, B) and continuous flow (C, D).

due to the much longer cycle lengths in fed-batch mode (3 days) compared to a shorter HRT (8 h) in continuous flow [16]. CEs ranged from 11 to 77% in batch mode, and from 4 to 82% in continuous flow operation, depending on resistance used as this affected the current density (Fig. 4B and D). There was a general decrease in CE in continuous mode compared to fed-batch mode, likely due to oxygen diffusion in the anodic chamber [28]. During continuous operation mode there was also a change in the leading CE performance. At the lowest external resistances R3 and R8 had the highest CE during fed-batch mode, whereas R5 was the best performer in continuous mode for this parameter.

3.3. Internal resistance

Total internal resistance was calculated from EIS and LSV measurements under fed-batch conditions. Individual components of internal resistance were identified for all configurations using EIS (Fig. S3). The sum of these constituents was compared to the total internal resistance obtained through LSV [17]. EIS measurements indicated an increase in total resistivity with the number of brushes, with 28 Ω cm for R3, 38 Ω cm for R5 and 55 Ω cm for R8 (Fig. 5). This increase in resistivity with brush number was also calculated based on LSV results, with differences <15% between the two methods for the R3, R5 and R8 configurations. Summed total resistances obtained for the R3, R5 and R8 configurations by EIS were in good agreement with the total resistance based on LSV. However, for the R8C configuration, the impedance calculated by LSV was almost 80% larger than that measured by EIS. The observation that power densities obtained with R8C were higher than those of R3 suggests that the slopes obtained from LSV data did not accurately reflect internal resistance.

Diffusion resistance was the main contributor (>61%) to total impedance for all configurations. Solution resistance increased with the number of brushes for the R3, R5 and R8 configurations, indicating that wider spacing between the edge of the brush and the cathode effectively increased electrode spacing [15] despite all brushes having the same spacing based on the brush core distance. Charge transfer resistance was the smallest component of impedance, but it was larger for R3 than for the other two configurations with more anodic current collectors (carbon brush metal core). Higher total internal impedance was responsible for lower currents and power densities in batch mode. The largest resistivity (R8 = 55 Ω cm) produced the smallest power density (600 mW m^{-2}), whereas the lowest total internal resistivity (R3 = 28 Ω cm) produced the highest power density (1270 mW m^{-2}).

3.4. Electrode spacing

To demonstrate that the change in distances between the edges of the anodes and cathodes affected the power densities produced by the smaller and larger brushes (and not just the brush size), the

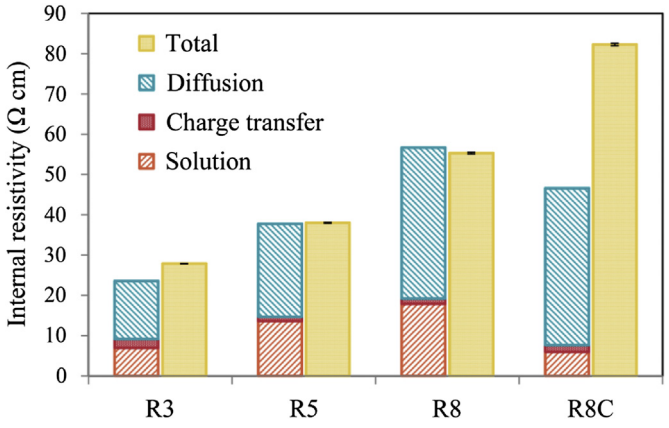

Fig. 5. Individual components of internal resistance based on EIS and total impedance based on slope of LSV tests for the four configurations under fed-batch mode.

anodes in the R8 configuration were moved closer to the cathode (from 12 to 4 mm, Table 1) (R8C) to produce the same spacing between the brush edges and the cathode as configuration R3. Power density substantially increased in both fed-batch and continuous mode, making this new smaller brush configuration with closer spaced electrodes (R8C) the best performer. The maximum power in fed-batch mode was 1030 mW m^{-2} (R8C) compared to 600 mW m^{-2} (R8) (Fig. 6A). In continuous flow, the maximum power was 1020 mW m^{-2} (R8C) compared to 280 mW m^{-2} (R8) (Fig. 6C). The observation that the R8C brushes performed better than the R3 brushes also shows that the brush total surface area is less important than average brush distance from the cathode.

Electrode potential curves (Fig. 6B and D) showed that cathode potentials were more stable in configuration R8C than in the previous R8 tests. EIS and LSV analyses were consistent with this trend in increased power with the closer electrode spacing. There was a substantial decrease in all impedance components for R8C compared to R8, with the solution resistance (directly related to electrode spacing) having the largest decrease by 84%, followed by a large reduction in diffusion resistance (51%) (Figs. 3 and 6).

The maximum power density with the R8C configuration was lower than that originally obtained using the R3 configuration (Fig. 3). However, more than a year had elapsed since that first series of tests, and power production by reactors can decrease over time due to cathode aging, as the performance of Pt-catalyzed cathodes decreases over time [29,30]. Therefore, an additional polarization test was done with the R3 configuration at the same time as the R8C experiments (R3-2, results shown in Fig. S4). In this second series of tests the R3-2 results showed significantly lower power densities (690 mW m^{-2} in fed-batch mode and 540 mW m^{-2} in continuous flow) than those obtained with the R8C (1030 mW m^{-2} in fed-batch mode and 1020 mW m^{-2} in continuous flow). This comparison of the R3-2 and R8C reactors at this time shows that the R8C reactor performed better than the R3-2 system even though the distance between the edge of the brushes and the cathode was the same for both (4 mm). The important difference here was that the distance between the cathode and the central axis of the brush (Ti current collector) was smaller for R8C (8 mm) than it was for R3-2 (17 mm). Therefore, it was concluded that electrode spacing based on the geometric center of mass of the anode had a significant effect on power generation.

The use of smaller brushes made possible to maintain closer electrode spacing on average, and would allow for a more compact design without the need of a separator. Shorter brush-anode diameters provide less distance along the graphite for electrons to get to the Ti current collector, decreasing internal resistance and increasing MFC performance. Smaller brushes also require less carbon fiber, with costs savings based on less materials used. Carbon brushes are well known to produce higher power densities in MFCs compared to carbon cloth or carbon felt, likely as a result of the high porosity [8,31]. It is possible that at some point the brushes could be too small to effectively produce more power than carbon cloth. The fact that power increased as the brushes were placed closer to the cathode in the R8C configuration also shows that oxygen transfer to the anode did not reduce power production, as it does when using flat anodes at that distance [15].

4. Conclusions

Polarization and power density curves showed substantial differences between brush anode configuration and operational regimes. For R3, power densities were 1240 mW m^{-2} in batch mode and 560 mW m^{-2} in continuous mode. For R8, these values were 690 mW m^{-2} in fed-batch mode and 280 mW m^{-2} in continuous flow. When the electrode spacing between the cathode and the

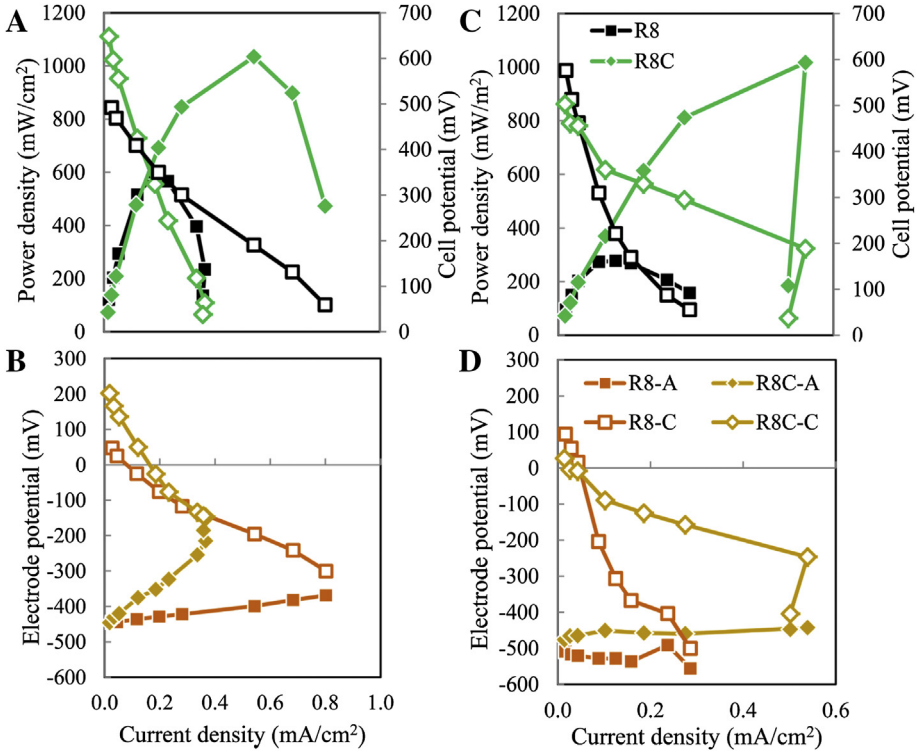

Fig. 6. (A and C) Power density (solid symbols) and polarization curves (white symbols) obtained through the single-cycle method for the two configurations: R8 (□) and R8C (◇). (B and D) Electrode potential curves (A = anode, solid symbols; and C = cathode, white symbols) measured against a reference electrode (Ag/AgCl). The curves were obtained in fed-batch (A, B) and continuous flow (C, D) operation.

central axis of the brush anode was decreased for R8 from 17 mm to 4 mm (configuration R8C), power density increased significantly in both fed-batch (1030 mW m^{-2}) and continuous mode (1020 mW m^{-2}). Based on the better performance of the smaller brushes in the R8C configuration compared to the R3 configuration (same electrode edge distance) in continuous flow conditions, we conclude that the location of the geometric center of mass of the anode also had a significant effect on power generation. The use of the smaller brushes may also have the benefit of a larger number of current collectors (i.e. 8 wires compared to 3 wires). A reduced brush diameter will enable the design of more compact reactors, without the need for a separator assembly, under continuous flow conditions.

Acknowledgments

The research reported here was financially supported by the King Abdullah University of Science and Technology in Saudi Arabia, and by the Strategic Environmental Research and Development Program (SERDP).

Appendix A. Supplementary data

Supplementary data related to this article can be found at http://dx.doi.org/10.1016/j.jpowsour.2013.08.110.

References

[1] B.E. Logan, Environ. Sci. Technol. 38 (2004) 160A–167A.
[2] K. Rabaey, W. Verstraete, Trends Biotechnol. 23 (2005) 291–298.
[3] D.R. Lovley, Nat. Rev. Microbiol. 4 (2006) 497–508.
[4] B.E. Logan, K. Rabaey, Science 337 (2012) 686–690.
[5] R.A. Rozendal, H.V.M. Hamelers, K. Rabaey, J. Keller, C.J.N. Buisman, Trends Biotechnol. 26 (2008) 450–459.
[6] B.E. Logan, Appl. Microbiol. Biotechnol. 85 (2010) 1665–1671.
[7] M. Zhou, M. Chi, J. Luo, H. He, T. Jin, J. Power Sources 196 (2011) 4427–4435.
[8] B. Logan, S. Cheng, V. Watson, G. Estadt, Environ. Sci. Technol. 41 (2007) 3341–3346.
[9] D. Jiang, X. Li, D. Raymond, J. Mooradain, B. Li, Int. J. Hydrogen Energy 35 (2010) 8683–8689.
[10] H. Liu, S. Cheng, L. Huang, B.E. Logan, J. Power Sources 179 (2008) 274–279.
[11] A. Dekker, A.T. Heijne, M. Saakes, H.V.M. Hamelers, C.J.N. Buisman, Environ. Sci. Technol. 43 (2009) 9038–9042.
[12] J.K. Jang, T.H. Pham, I.S. Chang, K.H. Kang, H. Moon, K.S. Cho, B.H. Kim, Process Biochem. 39 (2004) 1007–1012.
[13] B. Min, B.E. Logan, Environ. Sci. Technol. 38 (2004) 5809–5814.
[14] H. Moon, I.S. Chang, J.K. Jang, B.H. Kim, Biochem. Eng. J. 27 (2005) 59–65.
[15] S. Cheng, H. Liu, B.E. Logan, Environ. Sci. Technol. 40 (2006) 2426–2432.
[16] Y. Ahn, B.E. Logan, Appl. Microbiol. Biotechnol. 93 (2012) 2241–2248.
[17] A.J. Hutchinson, J.C. Tokash, B.E. Logan, J. Power Sources 196 (2011) 9213–9219.
[18] Y. Feng, Q. Yang, X. Wang, B.E. Logan, J. Power Sources 195 (2010) 1841–1844.
[19] S. Cheng, H. Liu, B.E. Logan, Electrochem. Commun. 8 (2006) 489–494.
[20] S. Cheng, D. Xing, D.F. Call, B.E. Logan, Environ. Sci. Technol. 43 (2009) 3953–3958.
[21] Y. Hong, D.F. Call, C.M. Werner, B.E. Logan, Biosens. Bioelectron. 28 (2011) 71–76.
[22] V.J. Watson, B.E. Logan, Electrochem. Commun. 13 (2011) 54–56.
[23] B.E. Logan, B. Hamelers, R. Rozendal, U. Schröder, J. Keller, S. Freguia, P. Aelterman, W. Verstraete, K. Rabaey, Environ. Sci. Technol. 40 (2006) 5181–5192.
[24] D. Jiang, B. Li, Biochem. Eng. J. 47 (2009) 31–37.
[25] S.B. Velasquez-Orta, T.P. Curtis, B.E. Logan, Biotechnol. Bioeng. 103 (2009) 1068–1076.
[26] Z. He, N. Wagner, S.D. Minteer, L.T. Angenent, Environ. Sci. Technol. 40 (2006) 5212–5217.
[27] Z. He, F. Mansfeld, Energy Environ. Sci. 2 (2009) 215–219.
[28] S.E. Oh, J.R. Kim, J.-H. Joo, B.E. Logan, Water Sci. Technol. 60 (2009) 1311–1317.
[29] T. Saito, T.H. Roberts, T.E. Long, B.E. Logan, M.A. Hickner, Energy Environ. Sci. 4 (2011) 928–934.
[30] B. Wei, J.C. Tokash, G. Chen, M.A. Hickner, B.E. Logan, RSC Adv. 2 (2012) 12751–12758.
[31] Y. Ahn, B.E. Logan, Energy Fuels 27 (2012) 271–276.